



Supplement of

Secondary aerosol formation alters CCN activity in the North China Plain

Jiangchuan Tao et al.

Correspondence to: Jiangchuan Tao (taojch@jnu.edu.cn) and Nan Ma (nan.ma@jnu.edu.cn)

The copyright of individual parts of the supplement might differ from the article licence.

1 **Inversion method of Size-resolved Particle Activation Ratio (SPAR):**

2 When the DMA is charged with a negative voltage, those aerosols with a small range of electrical
 3 mobility (Z_P) can pass through the DMA. When the scan diameter is set as D_{pi} for the singly charged
 4 particles and the respective voltage of DMA is V_i ($i = 1, 2, \dots, I$), aerosol particles with an electrical
 5 mobility of $Z_{p,i}$ ($i = 1, 2, \dots, I$) can pass through the DMA and the observed N_{CCN} by CCN counter can
 6 be expressed as:

$$7 \quad R_i = \int_0^{\infty} G(i, x) A(x) n(x) dx \quad (S1)$$

8 where x is the scale parameter with the definition of $x = \log(D_{pi})$; $A(x)$ is the SPAR of a single particle
 9 for scale parameter x ; and $n(x) = dN/d\log D_p$ is aerosol PNSD that is the multiple charging corrected
 10 results from the measured aerosol PNSD. We define the kernel function $G(i, x)$, which is crucial to the
 11 algorithm, as:

$$12 \quad G(i, x) = \sum_{\nu=1}^{\infty} \phi(x, \nu) \Omega(x, \nu, i) \quad (S2)$$

13 where $\phi(x, \nu)$ is the probability of particles that are charged with ν charges at the scale parameter of
 14 x (Wiedensohler, 1988). Transfer function $\Omega(x, \nu, i)$ is the probability of particles that can pass
 15 through the DMA with ν charges at the scale parameter x (Knutson and Whitby, 1975). In this study,
 16 the maximum value of ν is 10.

17 The multiple charging corrections can be expressed as computing the $A(x_i^*)$, in which x_i^* is the
 18 predetermined scale parameter from the DMA. To get the numerical integration results of Eq. (9), the
 19 range of the diameter is $[x_{int,1}, x_{int,J}]$ and the diameter interval that is 1/50 of the measured diameter is
 20 used. For $x_{int,1}$, its mobility is the 50% higher than the mobility of x_i^* with single charge. For $x_{int,J}$, its
 21 mobility is the 50% higher than the mobility of x_i^* with ten charges. Thus, Eq. (S2) can be written as:

$$22 \quad R_i = \int_{x_{int,1}}^{x_{int,J}} G(i, x) A(x) n(x) dx = \Delta x_{int} \sum_{j=1}^J \beta_j G(i, x_{int,j}) A(x_{int,j}) n(x_{int,j}) \quad (S3)$$

23 where $\beta_j = \begin{cases} 0.5, & j = 1, J \\ 1, & \text{otherwise} \end{cases}$, $x_{int,j}$ is the j th ($j=1, 2, \dots, J$) parameter that locates at the parameter x_i and

24 x_{i+1} , and $A(x_{int,j}), j=1, 2, \dots, J$ is SPAR at scale parameter $x_{int,j}$, which is expressed as the linear
 25 interpolation of the values at the measured diameters:

$$26 \quad A(x_{int,j}) = A(x_{i(j)}^*) + P_{i(j)} (x_{int,j} - x_{i(j)}^*) \quad (S4)$$

27 where P_i is the slope of the linear interpolation result of the five diameters that are nearest to the
 28 predetermined scale parameter x_i .

29 Then by considering

$$30 \quad H_{ij} = \beta_j \Delta x_{\text{int}} G(i, x_{\text{int},j}) n(x_{\text{int},j}) \quad (\text{S5})$$

31 the equation (S3) can be rewritten as:

$$32 \quad R_i = \sum_{j=1}^J H_{ij} A(x_{\text{int},j}) \quad (\text{S6})$$

33 then

$$\begin{aligned}
 34 \quad R_i &= \sum_{j=1}^J H_{ij} \left[A(x_{i(j)}^*) + P_{i(j)} (x_{\text{int},j} - x_{i(j)}^*) \right] \\
 35 \quad &= \sum_{j=1}^J H_{ij} A(x_{i(j)}^*) + \sum_{j=1}^J H_{ij} P_{i(j)} x_{\text{int},j} - \sum_{j=1}^J H_{ij} P_{i(j)} x_{i(j)}^* \\
 36 \quad &= \sum_{k=1}^I \left(\sum_{j=1}^J H_{ij} \delta(i(j)-k) \right) A(x_k^*) \\
 37 \quad &+ \sum_{k=1}^I \left(\sum_{j=1}^J H_{ij} x_{\text{int},j} \delta(i(j)-k) \right) P_k \\
 38 \quad &- \sum_{k=1}^I \left(\sum_{j=1}^J H_{ij} \delta(i(j)-k) \right) P_k x_k^* \\
 39 \quad &= \sum_{k=1}^I Q_{ik} A(x_k^*) + \sum_{k=1}^I T_{ik} P_k - \sum_{k=1}^I Q_{ik} P_k x_k^* \quad (\text{S7})
 \end{aligned}$$

40 where the Dirac Function is:

$$41 \quad \delta(x) = \begin{cases} 0, & x \neq 0 \\ 1, & x = 0 \end{cases} \quad (\text{S8})$$

42 thus

$$43 \quad Q_{ik} = \sum_{j=1}^J H_{ij} \delta(i(j)-k) \quad (\text{S9})$$

$$44 \quad T_{ik} = \sum_{j=1}^J H_{ij} x_{\text{int},j} \delta(i(j)-k) \quad (\text{S10})$$

45 by letting the

$$46 \quad S_i = R_i - \sum_{k=1}^I T_{ik} P_k + \sum_{k=1}^I Q_{ik} P_k x_k^* \quad (\text{S11})$$

47 this equation is then expressed as

$$48 \quad S_i = \sum_{k=1}^I Q_{ik} A(x_k^*) \quad (\text{S12})$$

49 or

$$50 \quad \mathbf{S} = \mathbf{Q}\mathbf{A} \quad (\text{S13})$$

51 where S and A are $I \times 1$ vectors and Q is an $I \times I$ matrix. This matrix can be solved by using the non-
 52 negative least square method. Finally, the A(x) can be determined and the corresponding size-resolved
 53 SPAR that is multiple charging corrected can be calculated.

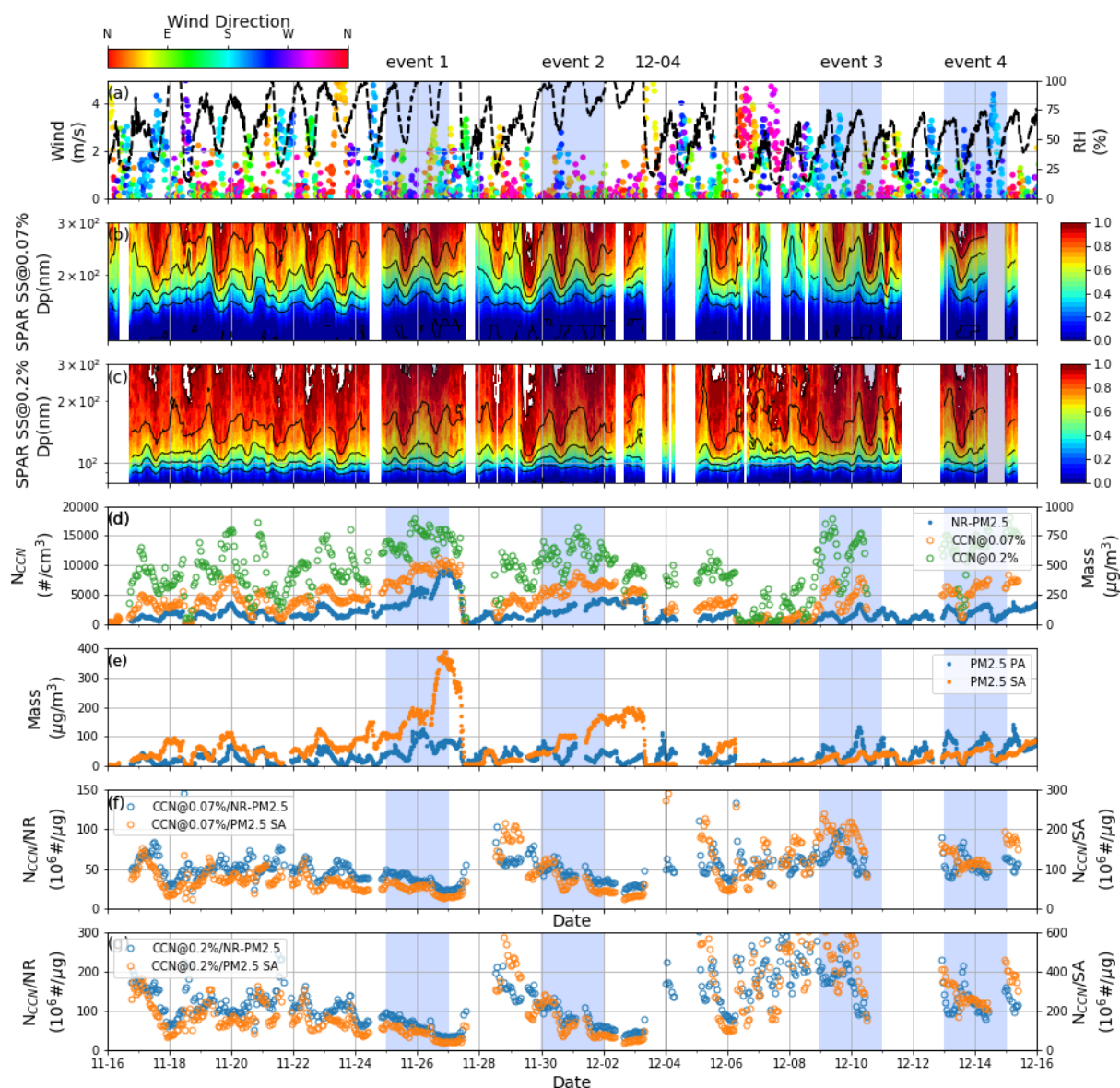
54

55 Reference:

56 Wiedensohler, A.: An approximation of the bipolar charge distribu- tion for particles in the submicron
57 size range, *J. Aerosol Sci.*, 19, 387–389, 1988.

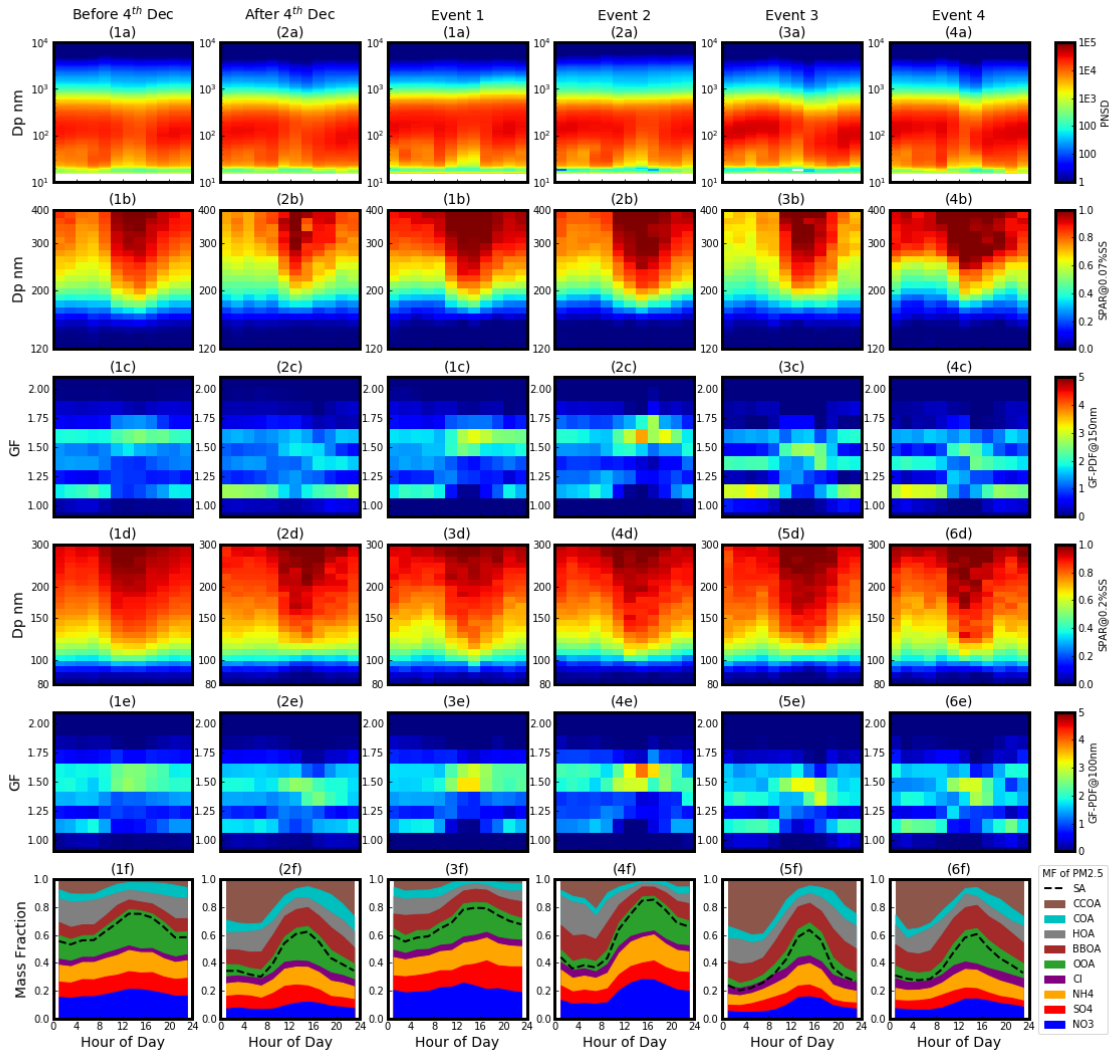
58 Knutson, E. O. and Whitby, K. T.: Aerosol classification by electric mobility: apparatus, theory, and
59 applications, *Jo. Aerosol Sci.*, 6, 443–451, 1975.

60



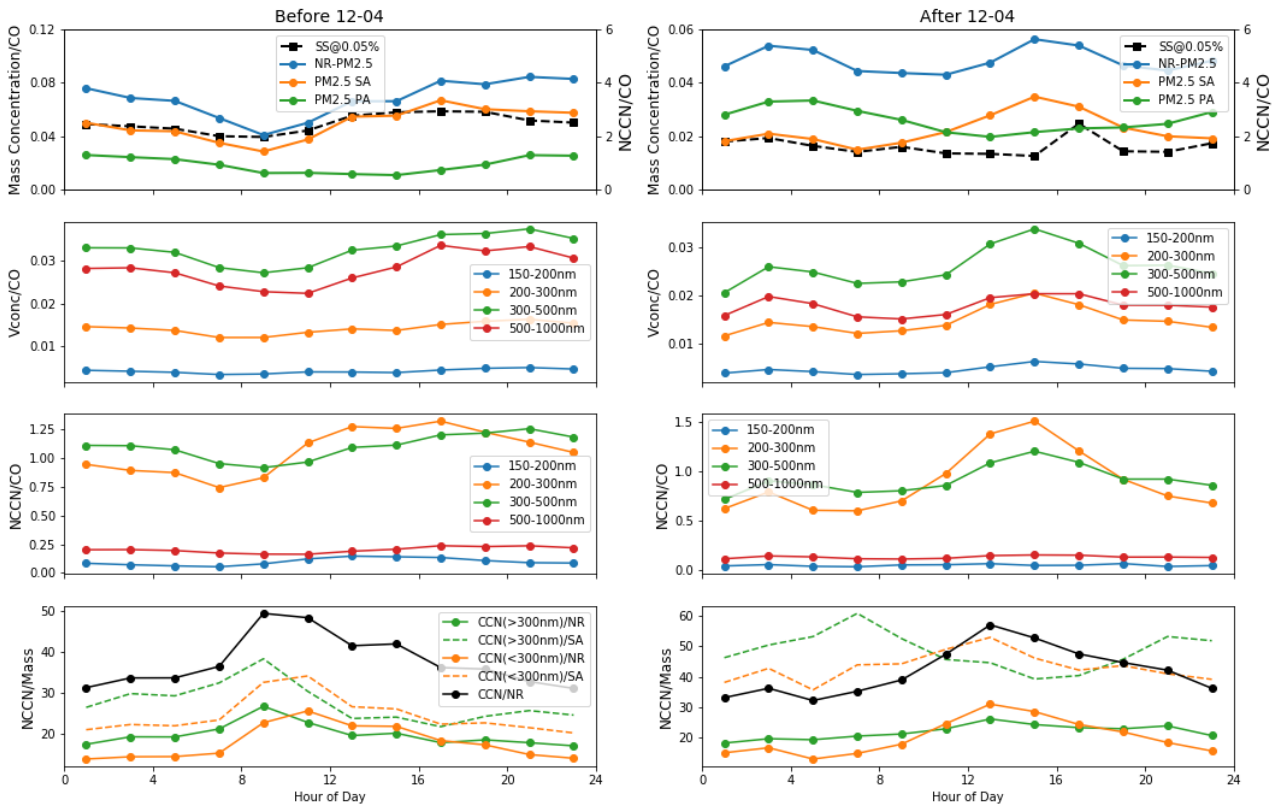
61

62 Fig S1. Overview of the measurements during the campaign: (a) dots represent wind speed with color
 63 indicating wind direction, and black lines represent RH; (b) SPAR under SS of 0.07%; (c) SPAR under
 64 SS of 0.2%; (d) blue, green and yellow dots represent NCCN under SS of 0.07% and 0.2%, and mass
 65 concentration of NR-PM_{2.5}, respectively; (e) blue and yellow dots represent mass concentration of
 66 PM_{2.5} PA and PM_{2.5} SA respectively; (f) blue and yellow dots represent ratio between NCCN at SS
 67 of 0.07% and mass concentration of NR-PM_{2.5} and PM_{2.5} SA, respectively. (g) blue and yellow dots
 68 represent ratio between NCCN at SS of 0.2% and mass concentration of NR-PM_{2.5} and PM_{2.5} SA,
 69 respectively. There were four events with significant enhancements of NCCN during the blue shaded
 70 periods.



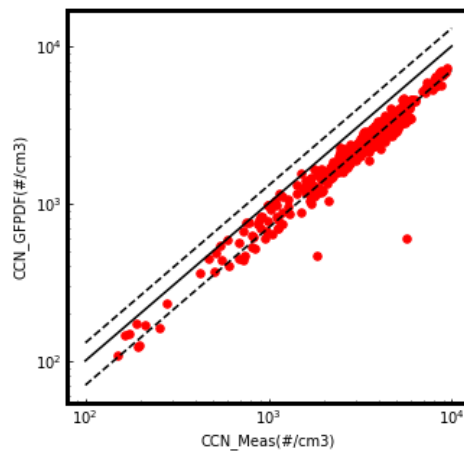
71

72 Fig S2. Diurnal variation of (a) PNSD, (b) SPAR at SS of 0.07%, (c) GF-PDF at 150nm, (d) SPAR at
 73 SS of 0.2%, (e) GF-PDF at 100nm and (f) mass fraction of different PM_{2.5} chemical species during
 74 high RH periods before 4th Dec (1) low RH periods after 4th Dec (2) and the four events (3-6), including
 75 OA factors: hydrocarbon-like OA (HOA), cooking OA (COA), biomass burning OA (BBOA), coal
 76 combustion OA (CCOA), and oxygenated OA (OOA).



77

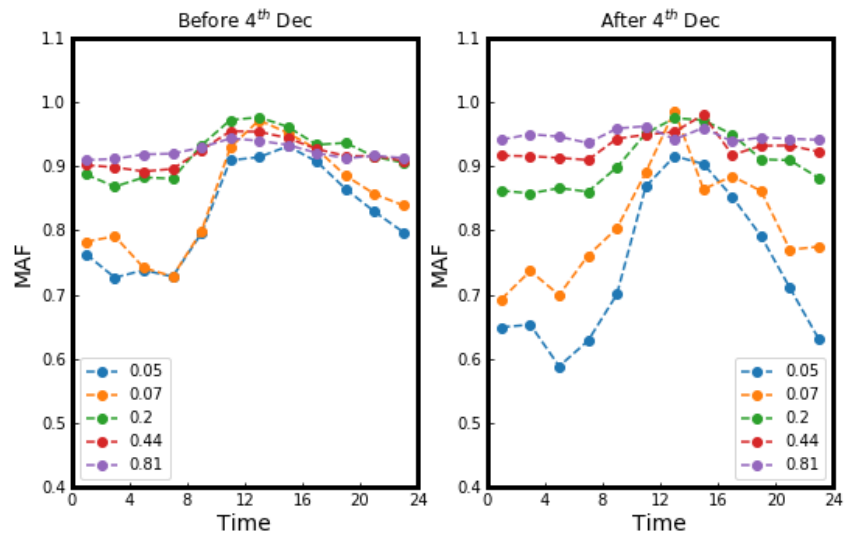
78 Fig S3. The same as Figure 4 but for periods before and after 12-04.



79

80 Figure S4. Comparison between the calculated NCCN based on GF-PDF and the measured NCCN.

81



82

83 Figure S5. Diurnal variations of MAF at the five measured SSs (indicated by different colors) during
 84 the high (left) and low (right) RH periods.